energies

MDPI

Article

Development of Magnetostrictive Transducer Prototype for Blockage Detection on Molten Salt Pipes

Héctor Andrés-Mayor, Miguel J. Prieto, Pedro J. Villegas, Fernado Nuño, Juan A. Martín-Ramos and Alberto M. Pernía *

Department of Electrical Engineering, University of Oviedo, 33203 Gijón, Asturias, Spain; hector.andres@eu4m.eu (H.A.-M.); mike@uniovi.es (M.J.P.); pedroj@uniovi.es (P.J.V.); fnuno@uniovi.es (F.N.); jamartin@uniovi.es (J.A.M.-R.)

* Correspondence: amartinp@uniovi.es; Tel.: +34-985-182566

Received: 5 February 2018; Accepted: 5 March 2018; Published: 8 March 2018

Abstract: In solar thermal power plants molten salt is often used to store and transport the energy that is collected during the day. The external pipe temperature is measured to activate an electric heating system if the temperature approaches the melting point. However, salt solidification cannot be completely excluded from the plant management. Once occurred, the location of a salt blockage is very complex due to the high temperature of the pipe. Therefore, when this problem arises, power plants have to stop production with the consequences in time and cost that this entails. Electro-magnetic acoustic transducers can be used as non-destructive testing systems for this application. A method for salt blockage detection is proposed that is applicable in straight sections of pipes by employing torsional guided waves that are generated with magnetostrictive transducers. The present paper deals with the transducer conception and the design of the power supply to activate it. Two alternatives are proposed and compared to determine the improvement in the amplitude/noise ratio. Finally, the experimental results show the performance of the equipment in a small prototype, thus validating the technique presented.

Keywords: guided waves; torsional waves; magnetostriction; electromagnetic acoustic transducer; electromagnetic acoustic transducer (EMAT); nondestructive testing; nondestructive testing (NDT); solar power plant

1. Introduction

Conventional solar thermal power plants (Figure 1) concentrate sun radiation to heat a transfer fluid (HTF) to high temperatures. This HTF is then transported to a thermodynamic cycle, commonly water-steam, to produce electricity through a steam turbine. Solar thermal plants can be classified according to their HTF operating temperature:

- Low temperature, below 200 °C, which can be found in household levels.
- Medium temperature, between 200 °C to 400 °C, as in Fresnel reflectors and parabolic troughs power plants.
- High temperature, above 400 °C, as in Stirling dishes and tower power plants.

A variety of fluids have been tested to transport the heat, including water, air, oil, and sodium. However, a molten salt is nowadays considered to be the most suitable solution [1]. It provides a low-cost means to store thermal energy, it is a liquid at atmospheric pressure, its operating temperatures are compatible with today's steam turbines, and it is non-flammable and nontoxic. Molten salt is also

used for energy storage in order to produce electricity at night or on overcast days, thus allowing for the use of solar power for baseload generation as well as peak power generation.

The eutectic solution KNO_3-$NaNO_3$, 54% and 46% ratio in weight, respectively, is one of the commonly used mixtures. Its usage is conditioned by its melting point, 222 °C, below which the salt becomes solid. That must be prevented at any cost.

Figure 1. Molten salt tanks for storing thermal energy in the solar plant "La Africana" Granada.

That is the reason why the external pipe temperature is measured at regular intervals in order to activate an electric heating system if necessary. However, solidification is a risk that cannot be completely excluded from the power plant management. Problems, such as a malfunction of the electric heating system or its misplacement, especially during start-up, can lead to salt solidification.

Additionally, the salt solution also stratifies, causing unbalance in the mixture. Measurements in a real plant (Figure 2) show that there is a temperature profile in the cross-section of the pipes of up to 30 °C of difference in the inside of a 15-inch-diameter pipeline (Table 1). Salt temperature is measured in the middle of the pipe's cross section (A). The temperature of the salt in contact with the interior of the pipe is estimated by thermocouples (B, C, D, E) while considering an 8 °C drop on the pipe wall.

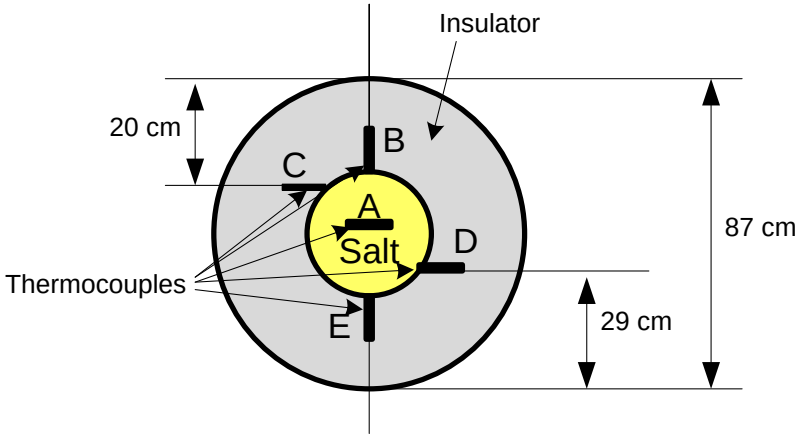

Figure 2. Cross section of the pipe and thermocouples position.

Table 1. Temperature measurements in molten salt pipes of the solar plant "La Africana".

Thermocouple Measure	Salt Temperature	External Temperature
TT-13WSX30CT001-JTC1position A	312.25 °C	
Thermocouple position B	294 °C	286 °C
Thermocouple position C	290 °C	282 °C
Thermocouple position D	285 °C	277 °C
Thermocouple position E	281 °C	273 °C

In addition, because it is a eutectic solution, the variation in the mixture due to the stratification entails a higher melting point than the one expected for the initial mixture [1].

Once it has occurred, removing a salt blockage is very complex. As salt density decreases with temperature [1], if heat is applied in the middle of the blockage the molten salt would expand, pressing outwards, and probably bursting the pipe. Objectively, this is very dangerous for the staff in the surroundings due to the low viscosity of the flowing fluid, its high temperature and its high energy coefficient. As a consequence, the safe procedure implies waiting until the temperature is low enough to replace the affected section in the pipeline, which results in paralyzing the power plant for approximately one week. This time could be reduced if the location and the borders of the blockage could be exactly determined at high temperature. In any case, the position of the blockage is always of interest. Once the blockage is located, then it can be heated from one end in order to melt it without danger.

Several techniques can be used to detect the blockage. As indicated above, thermocouples can be used to run tests that allow for temperature drops to be detected. However, these are local tests and will require either a large array of temperature sensors installed or local measurements every few meters with the resulting waste of time. Note that pipes in solar thermal power plants are insulated with one or several layers (Figure 2), which means that thermocouples should be included along the pipe and left there until they are needed. Radiometric tests (Figure 3) can also be used to detect the liquid-solid interface in the pipe. Again, these are local tests that also evince the aforementioned problems. Radiometric tests also require safety features, such as a clear area to perform the measurements as well as qualified personnel. One interesting technique is the use of acoustic waves, in especial the use of guided wave testing (GWT). GWT allows the inspection of sections of pipes several meters long. The technique has already been used to detect certain defects in pipes, such as cracks or corrosion. In the bibliography consulted, no previous research on the detection of salt blockage with GWT that is generated by magnetostrictive transducers has been found.

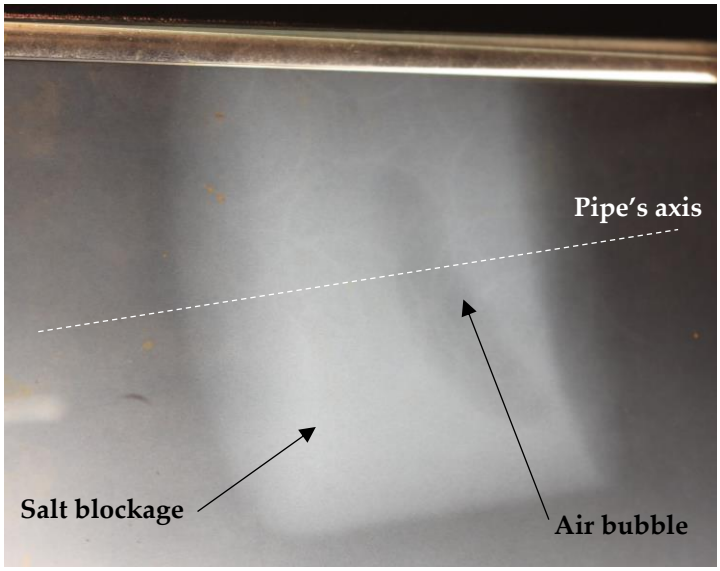

Figure 3. Lateral view of a scintigraphy from a salt blockage inside a test pipe.

The present paper describes a research in progress to detect the salt blockage at operating temperatures with magnetostrictive transducers that generate and detect guided waves.

2. Guided Wave Testing

GWT is a non-destructive test (NDT) that employs mechanical stress waves, which are characterized by relatively low frequencies (typically under 200 kHz). These waves propagate along elongated structures (e.g., rods, pipes and plates) while guided by the boundaries of such structures, and their behaviour is modified with respect to their free propagation in the bulk material. This technique has been specially used in pipes due to its advantages for long distance and reduced time tests.

Guided waves are characterised by their discretization into propagating modes, of which only a finite number are permitted for a given frequency, and by the existence of dispersion, which is the nonlinear relationship between wavenumber and frequency. The different solutions for a guided wave in a cylindrical material are defined by the following general forms for the displacement vector ($\hat{u}$) (1) and stress tensor ($\hat{\sigma}$) (2):

$$\hat{u}(r,\ \theta,\ z) = \widetilde{u}(r,\ \theta)e^{jkz} = u(r)e^{jn\theta}e^{jkz} \tag{1}$$

$$\hat{\sigma}(r,\ \theta,\ z) = \widetilde{\sigma}(r,\ \theta)e^{jkz} = \sigma(r)e^{jn\theta}e^{jkz} \tag{2}$$

where $(r,\ \theta,\ z)$ are the coordinates and (e_r, e_θ, e_z) the unit vectors in the cylindrical system, harmonic variation $e^{-j\omega t}$ is assumed, ω is the angular frequency, k the wavenumber, and integer n is a separation constant called the circumferential order, which determines the symmetry of the solutions in the azimuthal direction.

According to this symmetry, wave modes are classified in families. Those which have no dependence on the azimuthal coordinate θ, called axisymmetric modes $(n = 0)$, and those with dependence, called antisymmetric modes $(n \geq 1)$. In general, multiple propagating modes exist for a given circumferential order and frequency, so a second index m is used to sort them out. Following the convention that was used by Silk and Bainton [2], the first number is the circumferential order n and the second one the index counter m. Therefore, the axisymmetric modes are further divided into torsional waves $T(0, m)$ which only involve the azimuthal component and longitudinal waves $L(0, m)$ with both radial and axial components. Antisymmetric modes are labelled flexural waves $F(n, m)$ and involve all three components of the displacement vector. (Figure 4) shows the dispersion curves and the different wave modes in an aluminium pipe of Ø40 mm and 1.5 mm thickness. This figure has been obtained using PCdisp (Pochhammer-Chree dispersion) [3], which is a toolbox of Matlab routines that numerically simulates the generation and propagation of waves in a cylindrical waveguide.

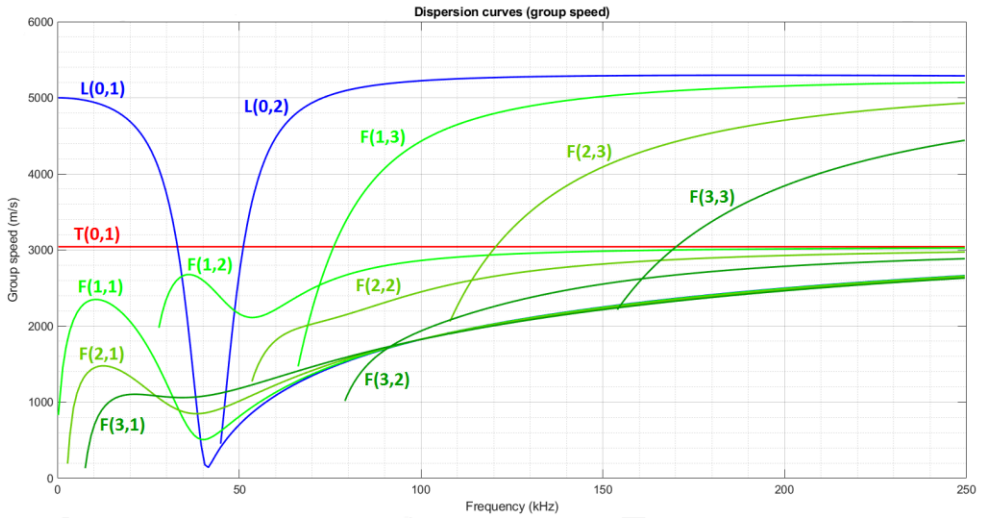

Figure 4. Group speed for the main wave modes in an aluminium pipe of Ø40 mm and 1.5 mm thickness.

The torsional mode T(0,1) has been highlighted due to its non-dispersive characteristics [4] and because it is the only torsional mode at low frequencies. There are extensive studies on the use of the torsional guided wave (TGW) technique, first introduced by Rose [5,6]. This technique has also been studied for sludge and blockage detection due to the interest arisen in different industries [7]. TGW equipment commonly consists of inflatable rings equipped with transducers modules based on piezoelectric effect generating torsional waves. Conventional TGW equipment with piezoelectric transducers can be used on pipes up to 150 °C, although improvements have been made to withstand up to 400 °C for a few minutes [8]. Therefore, equipment able to withstand high temperatures for an extended time is nowadays out of range for piezoelectric transducers.

TGW has also been successfully generated using Electromagnetic Acoustic Transducers, EMATs [9]. These devices can be divided into two categories: transducers based on the Lorentz Force [10] and transducers based on the magnetostrictive effect discovered by James Joule and its inverse effect (Villari effect) [11]. In turn, TGW can be produced with magnetostrictive transducers in either of two ways. One method consists in directly generating the guided wave in the material (if the pipe is made of a ferromagnetic material). The other one, uses a ferromagnetic patch attached to the pipe under test. In this second way, the mechanical tension is generated in the patch and is transmitted to the pipe using a couplant or a pure mechanical coupling, the latter being the objective of this investigation. One of the key features of the EMATs is the possibility to develop sensors that are capable of withstanding extreme temperatures for both cryogenic applications [12] and high-temperature environments, even for extended times. This is possible because the materials that are involved withstand these temperatures. As a counterpart, these transducers have a low conversion efficiency when compared to piezoelectrics [13]. EMATs have been developed and used to explore the inner and outer surface of long stretches of pipes looking for discontinuities, such as cracks or defects. This research aims to apply magnetostrictive transducers for blockage detection in the solar thermal industry

3. Test Equipment

3.1. Magnetostrictive Transducer

Several approaches have been taken for generating TGW with magnetostrictive transducers. Kwun [14] proposed a method to generate and detect them by using magnetostrictive effects with a nickel strip (a kind of ferromagnetic patch). This strip was attached to the pipe around its circumferential direction while an encircling solenoid coil was placed over it. Then, using permanent magnets, the strip was pre-magnetized to provide a bias magnetic field in the pipe under inspection. By doing so, torsional waves appear when an alternating current (AC) pulse is applied to the coil. If the magnitude of the pre-magnetization in the patch and the intensity of the magnetic field in the coil is not appropriate, unwanted waves, such as longitudinal or flexural waves, can be generated. The system has been further developed and tested in industrial environments [15]. Park [16] suggested another method to generate guided waves with a nickel strip that is attached to the pipe at 45° from the circumferential direction. By doing so, the magnetic field reaches the strips at the desired oblique angle in order to avoid the generation of unwanted waves, regardless of the input current magnitude. Vinogradov [17] and Yi-Gon Kim [18] also proposed a crossed-coil magnetostrictive sensor that was composed of a solenoid and a toroidal coil instead of a permanent magnet.

In this research, with the purpose to show the feasibility of the TGW technique with magnetostrictive transducers to detect blockages, we present a sensor based on Park's method. Several strips are attached on the pipe at 45° from the circumferential direction, which are activated by an encircling solenoid and two permanent magnets (Figure 5). Note that permanent magnets cannot stand high temperatures, and therefore in future research they will be replaced with a second coil operating as an electromagnet.

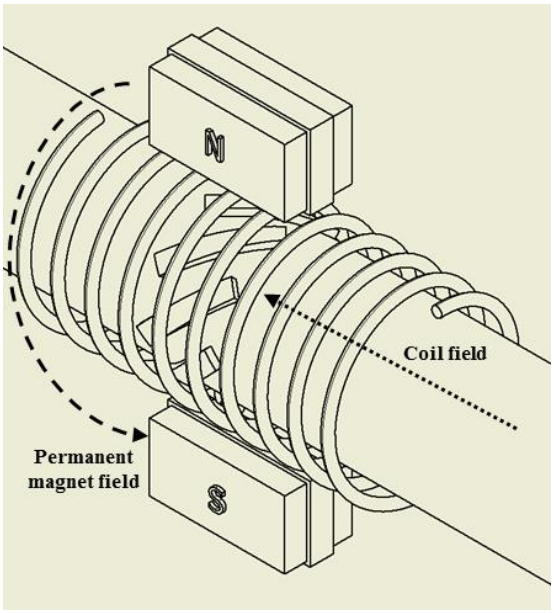

Figure 5. Magnetostrictive transducer design.

Magnetostrictive materials change their shape or dimensions during the process of magnetization. Therefore, in order to generate TGW, an alternative magnetic field (HAC) must be applied. The mechanical strain produced has the same sign regardless of the magnetization direction. In order to achieve a higher and more linear response, the HAC field should be applied when combined with a static magnetic field (HDC) located away from 0. As can be seen in Figure 6, the effect of the combined fields in point B is greater than the one in point A, where only HAC is applied.

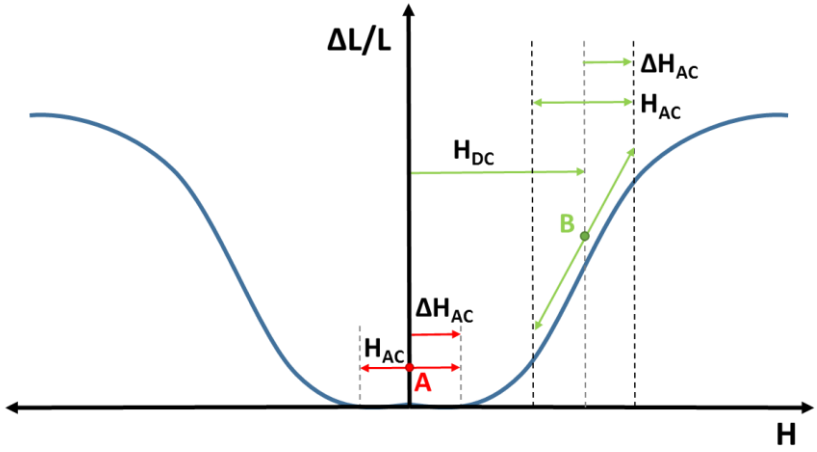

Figure 6. Typical magnetostrictive curve-related magnetic field (H) and mechanical strain (ΔL/L) [13].

In the present transducer, the permanent magnets create a static quasi-circular magnetic field (HDC) around the pipe, thus pre-magnetizing the strips. The dynamic magnetic field (HAC) is achieved by means of the encircling solenoid. As a result, a combined magnetic field is created along the strips in the direction that they are attached, thus generating the torsional wave pulse (Figure 7).

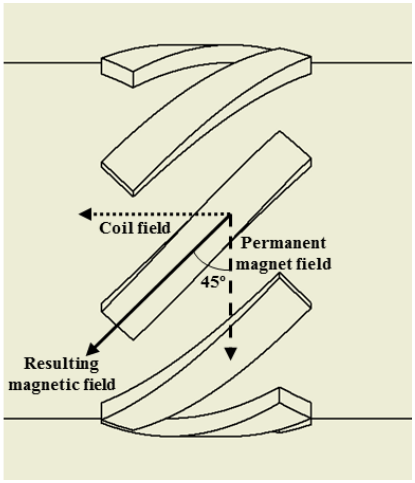

Figure 7. Resulting magnetic field on the strip.

Several magnetostrictive materials have been analysed for the transducer strips (Table 2). Permendur-2V (a cobalt-iron soft magnetic alloy) is selected due to its high elongation coefficient.

Table 2. Elongation coefficient of analysed magnetostrictive materials.

A. Elongation Coefficients	
Material	$\Delta L/L$
Nickel	-33×10^{-6}
45 Permalloy	27×10^{-6}
Vanadium Permendur	70×10^{-6}
Steel	21×10^{-6}

The strips have been mechanically coupled to the pipe. Although the use of a couplant might lead to better results, it will be difficult to use it at high temperatures. Thus, it has to be proven that a pure mechanical coupling can be used. In this case, for test purposes, adhesive tape is used because of its simplicity. For future research at high temperature, metallic clamps will be used.

The final transducer design involves eight permendur-2V strips around the pipe (Figure 8), which are surrounded by the coil and two NdFeB 50 × 25 × 10 mm permanent magnets symmetrically attached over the coil (Figure 5).

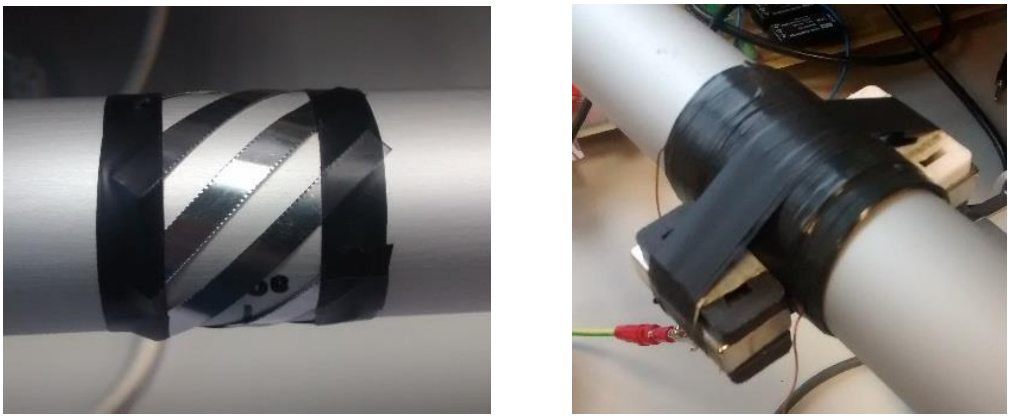

(**a**) (**b**)

Figure 8. (**a**) Permendur strips attached around the pipe at 45°. (**b**) Transducer with coil and magnets.

3.2. Power Supply and Instrumentation

To drive the transducer, a power supply is needed. Initially, a full-bridge based voltage power supply was used, as shown in Figure 9 (blue). The load is represented by an inductance and a small series resistance, which is the equivalent circuit of the solenoid, LS. To activate the transducer, a single positive voltage pulse is applied to the solenoid coil through the main full-bridge switches, Q1–Q4. As expected, a constant voltage produces an increasing current in the solenoid, Ch1 in Figure 10. The maximum current level is limited by reducing the input voltage value, Vin, which determines the value of the current slope. After 25 µs, the voltage pulse is finished and the transistors of the bridge are opened. The current in the solenoid is then derived through diodes D2–D3, which apply a negative voltage pulse across the sensor, Ch3 in Figure 10. The solenoid is then discharged. As a consequence, a triangular current waveform is applied to the solenoid. In the experiment results shown in Figure 10, Vin has been set to 50 V so as to obtain a maximum current of 18 A.

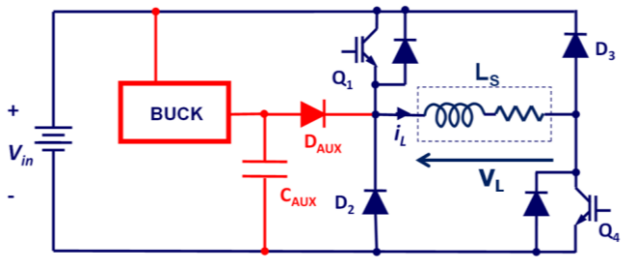

Figure 9. Final design of the power source.

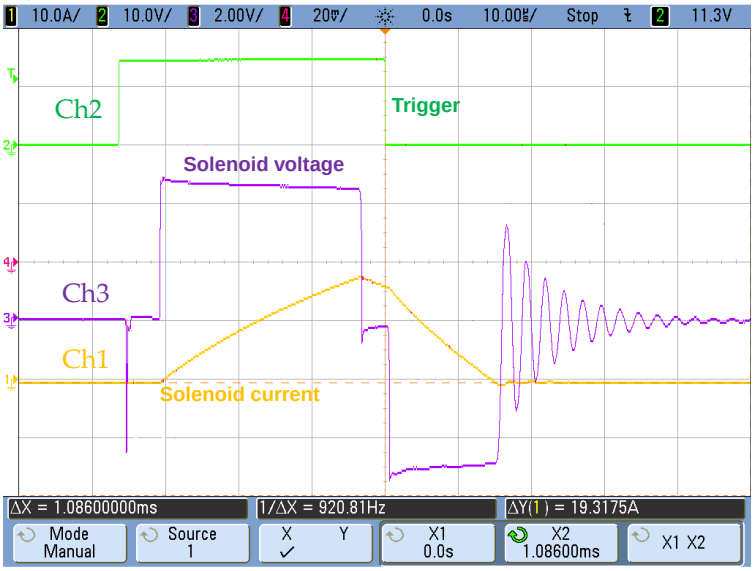

Figure 10. Waveforms at the solenoid. Ch1 represents solenoid current, Ch3 solenoid voltage, and Ch2 the trigger signal.

A triangular current waveform is a good alternative to activate the transducer; however, a new proposal for improving the signal/noise ratio is presented afterwards.

This power supply can be improved if an auxiliary buck converter is added to the bridge, as represented in Figure 9 (red). Now, a new stage can be added to the topology (Figure 11). First stage: Q1–Q4 are closed to produce the first current slope; second stage: Q1 is opened and Q4 remains closed, thus creating a constant-current period; third stage: all the switches are opened.

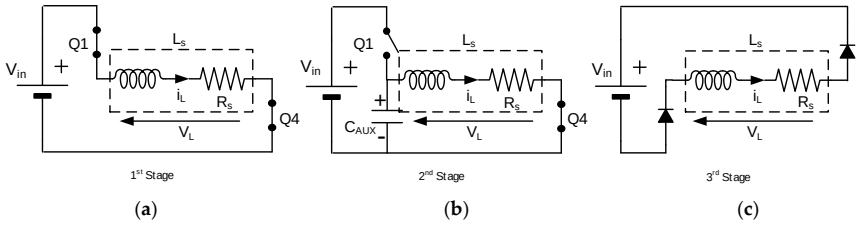

Figure 11. Full-bridge+buck converter stages: (**a**) First stage, (**b**) Second stage, (**c**) Third stage.

By including this additional stage, the input voltage, Vin, is used to control the maximum current slope, while the additional buck converter fixes the voltage value across the auxiliary capacitor, C_{AUX}, which will give rise to the constant current period. Since this voltage aims to compensate the decaying factor of the series resistance of the solenoid Rs, it must be calculated as a function of this series resistance and the desired current level. In Figure 12, the simulated main waveforms of this new scheme are shown. Since the bridge transistors Q1–Q4 are initially closed, and given that voltage Vin is above 300 V, the current through the solenoid reaches the set point, 30 A (in only a few microseconds, in this case). Then, Q1 is opened while Q4 is still closed. C_{AUX} is then connected to the solenoid through D_{AUX}, thus making the current through the solenoid almost constant, while the applied voltage slightly drops. Finally, Q4 is opened and the solenoid is discharged through D2 and D3. During the operation, the auxiliary capacitor is slightly discharged, and the buck converter is activated to recharge it.

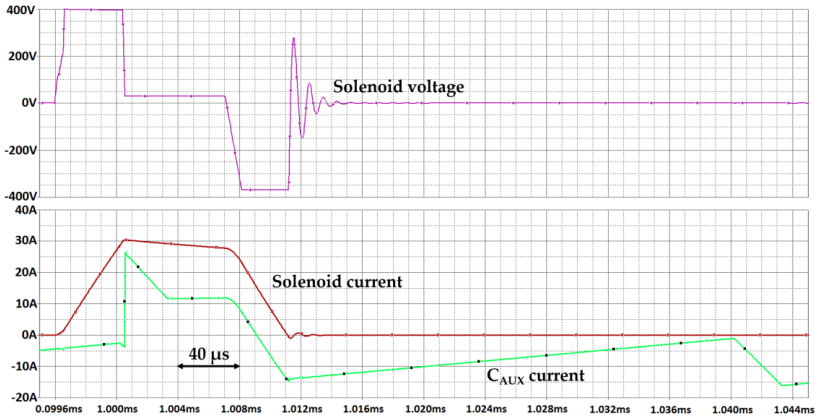

Figure 12. Simulated waveforms for the FB+buckpower supply.

A prototype version of the power supply can be seen in Figure 13.

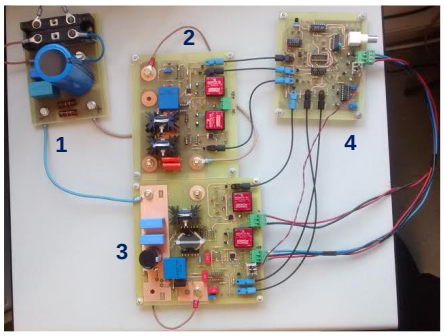

Figure 13. Experimental version of the power source. 1—Input rectifier. 2—Power bridge. 3—Auxiliar buck converter. 4—Control stage.

4. Results and Discussion

Operation Tests

With the purpose to show the feasibility of the technique, initial tests have been carried out on nonmagnetic pipes. The blockage inside the pipe has been simulated by solid cement. An 11-mm wide cement blockage is made on a 5 m long, Ø40 mm (outside diameter), and Ø37 mm (inside diameter) aluminium pipe. Two transducers are situated on the pipe, with one performing as emitter (Tx) and the other as receiver (Rx), as can be seen on Figure 14.

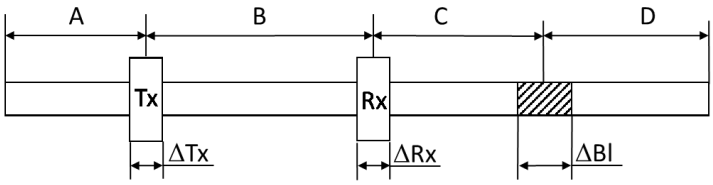

Figure 14. Test arrangement.

Distances for the first experiment are shown in Table 3, where the width of both, the transducers and the blockage, has been taken into consideration because of the uncertainty of the acoustic wave origin and the reflected echo respectively.

Table 3. First test distances.

Distance	Value	Unit
A	1000	
B	1000	
C	1955	
D	1045	mm
ΔTx	50	
ΔRx	50	
ΔBl	110	

The generated torsional wave in Tx (Figure 14) will travel along the pipe and will be altered by discontinuities in the pipe's material or in the adjacent matter. At each discontinuity interface, part of the acoustic wave will pass through and part will be reflected back. Thus, the main expected signals are the ones that are received directly from Tx to Rx, echo 1, and the echoes result of the acoustic wave reflected on the blockage, echo 3, and those that are reflected on the pipe's ends, echoes 2 and 4. (Table 4).

Table 4. Main expected echoes according to Figure 14.

Signal	Distance	
Echo 1	$B \pm \left(\frac{\Delta Tx}{2} + \frac{\Delta Rx}{2}\right)$	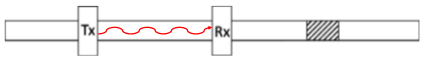
Echo 2	$A + A + B \pm \left(\frac{\Delta Tx}{2} + \frac{\Delta Rx}{2}\right)$	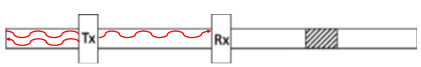
Echo 3	$B + C + C \pm \left(\frac{\Delta Tx}{2} + \frac{\Delta Rx}{2} + \frac{\Delta Bl}{2}\right)$	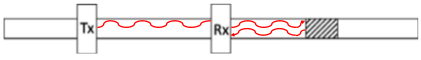
Echo 4	$B + C + D + D + C \pm \left(\frac{\Delta Tx}{2} + \frac{\Delta Rx}{2}\right)$	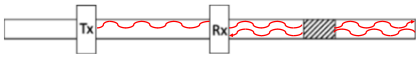

To compare the behaviour of both waveforms (triangular current, Figure 15, and trapezoidal current Figure 16), the transducer Tx is activated with a 5-A-peak and 12-µs-period current every 10 ms for both cases. The voltage that is applied in each power supply to the transducer (green) and the resulting current (purple) can be seen in the following figures:

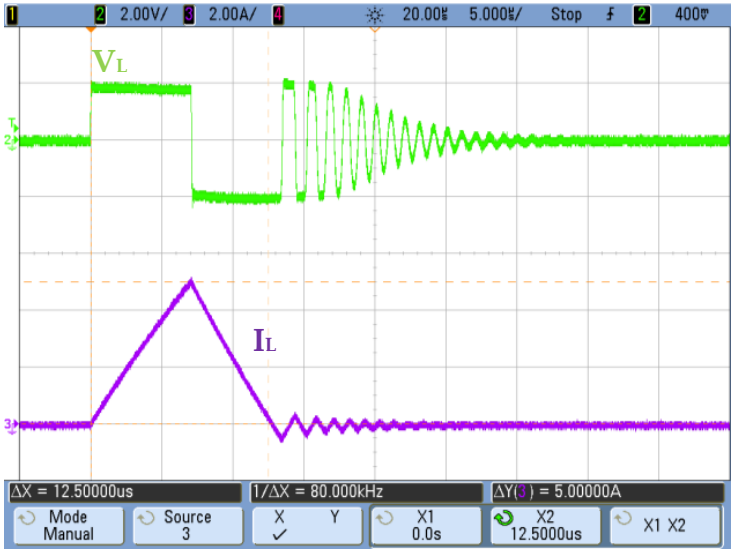

Figure 15. Triangular current (Channel 3, purple) and voltage pulse (Channel 2, green) applied to the transducer. Only full-bridge used.

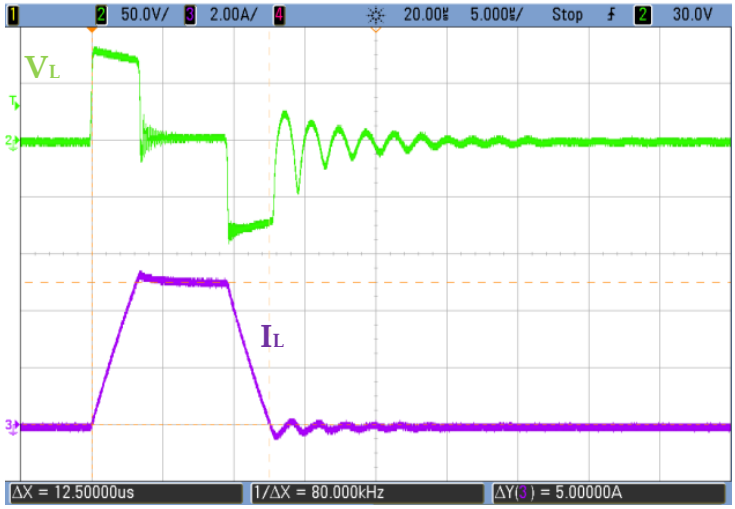

Figure 16. Trapezoidal current (Channel 3, purple) and voltage pulse (Channel 2, green) applied to the transducer by means of using full-bridge+buck converter.

The echoes that were sensed in the transducer Rx (Figure 14) are filtered and amplified previous to their visualization on the laboratory oscilloscope with an average filter. The resulting signal shows voltage peaks corresponding to the reflected echoes, as can be distinguished in Figure 17 for the full-bridge and in Figure 18 for the full-bridge+buck converter.

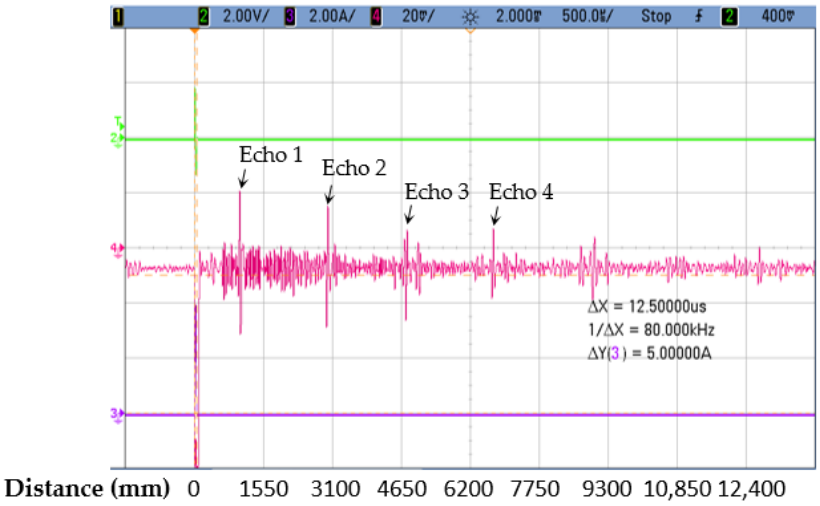

Figure 17. Received echoes using full-bridge (FB).

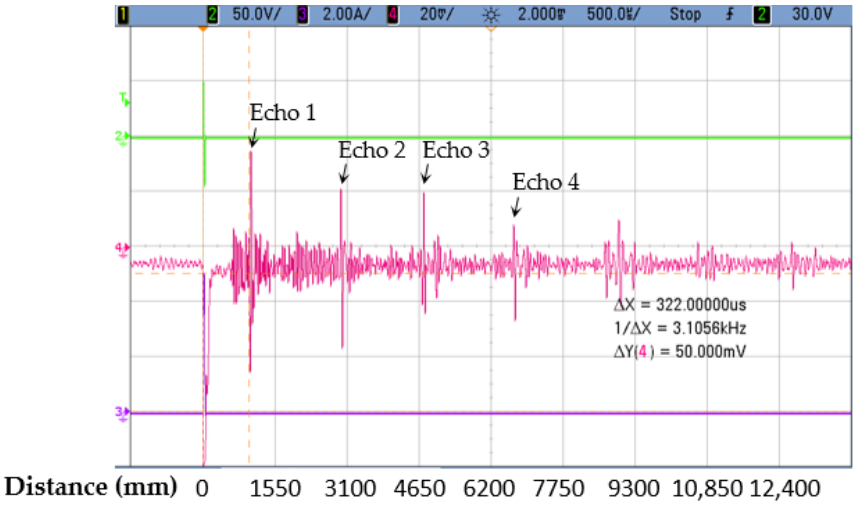

Figure 18. Received echoes using full-bridge+buck converter.

The distance travelled by each echo is estimated for a wave speed of 3120 m/s in the aluminium pipe (group speed of T(0,1) in Figure 4), leading to the experimental result shown in Table 5.

Table 5. Experimental results: Distance measurements.

Echo	Distance(mm)	Estimated Time (μs)	Measured Time (μs)		Error	
			FB	FB+buck	FB	FB+buck
Echo 1	1000 ± 50	320.5 ± 16	325	325	1.4%	1.4%
Echo 2	3000 ± 50	961.5 ± 16	965	955	0.36%	0.67%
Echo 3	4910 ± 105	1573 ± 34	1520	1530	3.36%	2.73%
Echo 4	7000 ± 50	2243 ± 16	2170	2160	3.25%	3.7%

The same test has been repeated several times for different positions of both transducers Tx and Rx, leading to similar results.

Both versions of the power supply have been compared experimentally in a range of frequencies from 30 kHz to 105 kHz by analysing the normalized signal amplitude in echo 1 (Figure 19), i.e., the ratio between the amplitude obtained at each frequency and the maximum amplitude obtained for that

echo. The two transducers are placed 1 m away from each other, and the results that were obtained show larger amplitudes when the FB-buck converter is used.

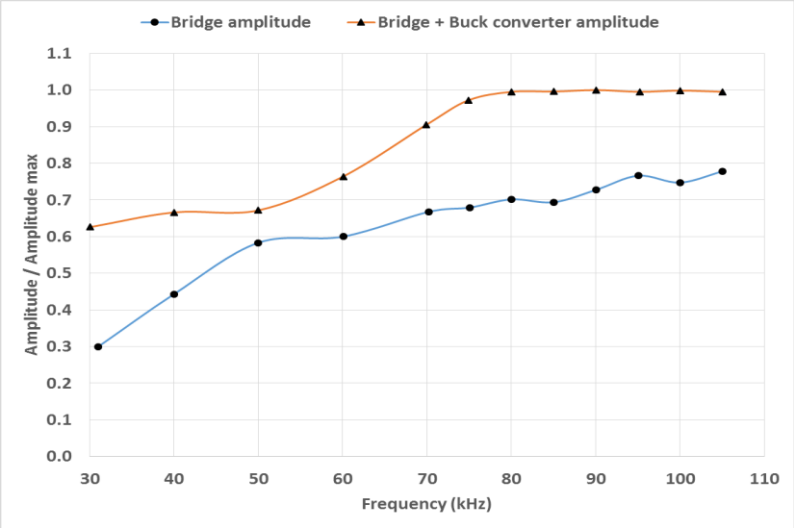

Figure 19. Signal amplitude for both FB and FB+buck converter vs pulse frequency.

Another important parameter to take into account is the ratio signal-amplitude/noise (Figure 20). The evaluation of the noise has been carried out using a window of 50 µs, where the average of the noisy signals amplitude is calculated. From the results obtained, the maximum signal-amplitude/noise ratio is very similar in both cases, but the amplifier that is required for triangular currents requires a higher gain. It can be also detected the optimum period (12 µs) for the FB+buck converter. As seen in Figure 19, different frequencies generate similar amplitudes but they have a different signal-amplitude/ratio (Figure 20). This optimal operating frequency is higher in the FB+buck when compared to the FB. A higher frequency dependence is also of interest for defining the transducer optimal operating point, which is related to the strip dimensions. The noise may be caused by the generation of other unwanted modes, as can be seen for the frequency range of the experiment in Figure 4.

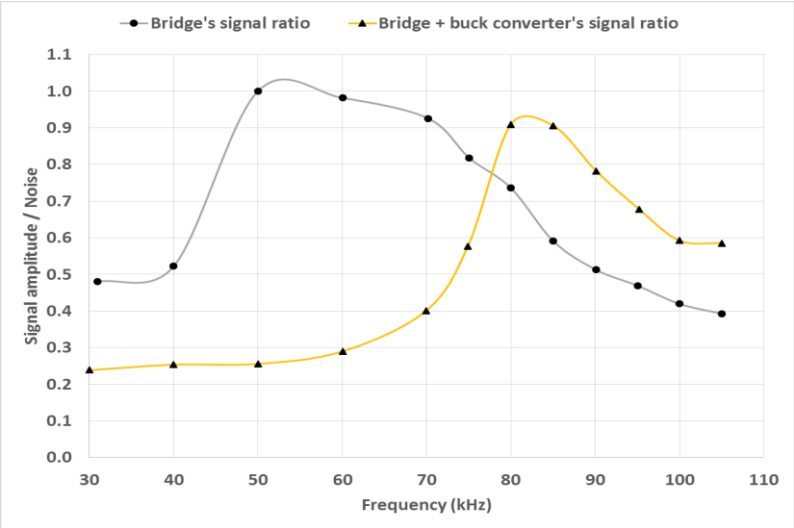

Figure 20. Signal/noise ratio for both FB and FB+buck converter vs pulse frequency.

As indicated in Section 3.1, permanent magnets cannot stand high temperatures. In future tests, a transducer with two encircling solenoids will be used. One coil is used to generate the alternative magnetic field and the other replaces the permanent magnets' static field. The new transducer and its preliminary tests are shown in Figure 21.

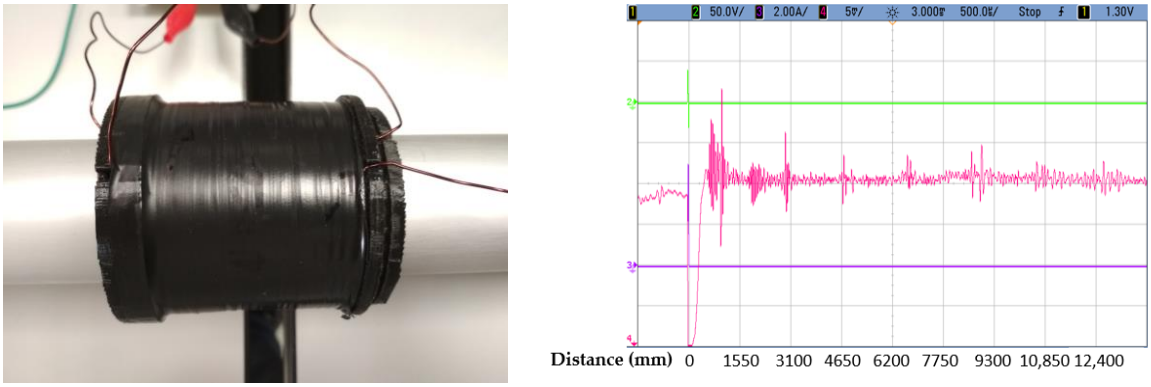

(**a**) (**b**)

Figure 21. (**a**) Transducer with two encircling solenoids (**b**) Preliminary results with the new transducer under the same test conditions as those in Figure 18.

5. Conclusions

A magnetostrictive transducer has been designed and assembled. The electromagnetic transducer is based on Permendur strips mechanically coupled at 45° and two magnets that give rise to a constant magnetic field polarization. Not using couplants is key to further developing the technique at high temperatures. Due to this, the signal/noise ratio is low and therefore the excitation signal has to be studied to improve performance. The power supply developed allows for the electromagnetic transducer to be supplied with a triangular or trapezoidal current. Both alternatives were tested to determine the maximum amplitude signal. It was observed that the triangular current shape generates lower signal amplitude in the echo received in the transducer. On the other hand, the maximum signal/noise ratio is very similar in both cases, but due to the lower signal amplitude with the triangular current, the amplifier that is used for this option should be designed to have a large gain.

The present research also proves experimentally the feasibility of using magnetostrictive transducers without couplants for detecting blockages in aluminium pipes at ambient temperature. Once the technique has been proved, further tests will be performed at high temperatures.

Acknowledgments: This research has been co-funded by the Plan of Science, Technology and Innovation of the Principality of Asturias through Project FC-15-GRUPIN14-122, and by the Spanish Government with the action TEC2016-77738-R.

Author Contributions: This paper is part of a research carried out by Alberto M. Pernía and Héctor Andrés-Mayor, whereas Juan A. Martín-Ramos and Pedro J. Villegas assisted with the electronic instrumentation and measurements. Fernando Nuño and Miguel J. Prieto contributed with the experimental measurements in the solar plant and the theoretical analysis of the torsional waves.

Conflicts of Interest: The authors declare no conflict of interest.

References

1. Bauer, T.; Laing, D.; Tamme, R. Overview of PCMs for Concentrated Solar Power in the Temperature Range 200 to 350 °C. *Adv. Sci. Technol.* **2010**, *74*, 272–277. [CrossRef]
2. Silk, M.G.; Bainton, K.F. The propagation in metal tubing of ultrasonic wave modes equivalent to Lamb waves. *Ultrasonics* **1979**, *17*, 11–19. [CrossRef]

3. Seco, F.; Jiménez, A.R. Modelling the generation and propagation of ultrasonic signals in cylindrical waveguides. In *Ultrasonic Waves*; InTech: Rijeka, Croatia, 2012.
4. Bertoncini, F.; De Lorenzo, G.; Giunta, G.; Raugi, M.; Turcu, F. Effect of Attenuation on Inspection Range and Sensitivity in Long-Range Guided Wave NDT of Coated and Buried Pipes. 2010. Available online: http://www.ndt.net/article/ndtnet/2010/16_TurcuRev1.pdf (accessed on 6 March 2018).
5. Rose, J.L.; Ditri, J.J.; Pilarski, A.; Rajana, K.; Carr, F. A guided wave inspection technique for nuclear steam generator tubing. *NDT E Int.* **1994**, *27*, 307–310. [CrossRef]
6. Ditri, J.J.; Rose, J.L. Excitation of guided elastic wave modes in hollow cylinders by applied surface tractions. *J. Appl. Phys.* **1992**, *72*, 2589–2597. [CrossRef]
7. Ma, J.; Lowe, M.J.S.; Simonetti, F. Feasibility study of sludge and blockage detection inside pipes using guided torsional waves. *Meas. Sci. Technol.* **2007**, *18*, 2629–2641. [CrossRef]
8. Charchuk, R.; Werstiuk, C.; Evans, M.; Sjerve, E. High Temperature Guided Wave Pipe Inspection. In Proceedings of the 4th International CANDU In-service Inspection Workshop and NDT in Canada 2012 Conference, Toronto, ON, Canada, 18–21 June 2012; pp. 18–21.
9. Hirao, M.; Ogi, H. *Electromagnetic Acoustic Transducers: Noncontacting Ultrasonic Measurements Using EMATs*; Springer: Tokyo, Japan, 2017.
10. Nakamura, N.; Ogi, H.; Hirao, M. Mode Conversion and Total Reflection of Torsional Waves for Pipe Inspection. *Jpn. J. Appl. Phys.* **2013**, *52*, 07HC14. [CrossRef]
11. William, R.C. Theory of Magnetostrictive Delay Lines for Pulse and Continuous Wave Transmission. *IRE Trans. Ultrason. Eng.* **1959**, *PGUE-7*, 16–32. [CrossRef]
12. Bertoncini, F.; Raugi, M.; Turcu, F. Application of Ultrasonic Guided Waves in the Field of Cryogenic Fluids. 2010. Available online: http://www.idspektr.ru/10_ECNDT/reports/1_13_12.pdf (accessed on 6 March 2018).
13. Kim, Y.Y.; Kwon, Y.E. Review of magnetostrictive patch transducers and applications in ultrasonic nondestructive testing of waveguides. *Ultrasonics* **2015**, *62*, 3–19. [CrossRef] [PubMed]
14. Kwun, H.; Sang-Young, K.; Crouch, A.E. Method and Apparatus Generating and Detecting Torsional Waves for Long Range Inspection of Pipes and Tubes. U.S. Patent 662,462,8B1, 23 September 2003.
15. Bertoncini, F.; Giunta, G.; Raugi, M.; Turcu, F. Overview and Experimental Evaluation of Magnetostrictive Transducers for Guided Wave Inspection. 2012. Available online: http://www.ndt.net/article/ndtnet/2012/1_Turcu.pdf (accessed on 6 March 2018).
16. Park, C.; Han, S.; Cho, S.; Kim, Y. *The Generation of Torsional Waves and the Pipe Diagnosis Using Magnetostrictive Transducers*; Transactions of the Korean Society for Noise and Vibration Engineering: Seoul, Korea, 2004; Volume 14, pp. 144–149.
17. Vinogradov, S. Method and System for the Generation of Torsional Guided Waves Using a Ferromagnetic Strip Sensor. U.S. Patent 7,573,261, 11 August 2009.
18. Kim, Y.-G.; Moon, H.-S.; Park, K.-J.; Lee, J.-K. Generating and detecting torsional guided waves using magnetostrictive sensors of crossed coils. *NDT E Int.* **2011**, *44*, 145–151. [CrossRef]